Effect of the interparticle potential on the yield stress of amorphous solids

Smarajit Karmakar, Edan Lerner, Itamar Procaccia, and Jacques Zylberg

Department of Chemical Physics, The Weizmann Institute of Science, Rehovot 76100, Israel

A crucially important material parameter for all amorphous solids is the yield stress, which is the value of the stress for which the material yields to plastic flow when it is strained quasistatically at zero temperature. It is difficult in laboratory experiments to determine what parameters of the interparticle potential affect the value of the yield stress. Here we use the versatility of numerical simulations to study the dependence of the yield stress on the parameters of the interparticle potential. We find a very simple dependence on the fundamental scales that characterize the repulsive and attractive parts of the potential, respectively, and offer a scaling theory that collapses the data for widely different potentials and in different space dimensions.

I. INTRODUCTION

At small external strain every solid reacts elastically. We are interested here in the response of amorphous solids to high external strains, and in particular in the yield stress σ_Y which cannot be exceeded without effecting a plastic response that typically leads to mechanical failure via plastic flow, shear banding, or fracture [1–3]. In this paper we focus on the fundamental microscopic features that determine the yield stress, using to great advantage the versatility of numerical simulations in which the interparticle potential can be varied at will. We work at zero temperature and quasistatic external straining conditions (the so-called athermal quasistatic or AQS limit) where very precise simulation results can be obtained. To introduce the issue we examine Fig. 1, which exhibits a typical stress vs strain curve, here for a system of $N = 500$ particles in AQS conditions. The yield stress is the average stress in the elastoplastic steady state that is obtained, say, after 100% deformation.

Clearly, the connection of the yield stress to the fundamental microscopic characteristics of the material is of great interest, but in fact far from being determined. To a large extent the determination of the yield stress of various amorphous solids is still a question of trial and error without much theoretical input. From the point of view of fundamental theory we have results for the dependence of the yield stress on the density $\tilde{\rho}$ only in the case of very simple interparticle potentials that are purely repulsive, without an attractive tail. Simple results are available for potentials of the form $\phi(r) \sim r^{-\alpha}$. Defining the rescaled (dimensionless) density as $\rho = \lambda^d \tilde{\rho}$ [where λ is a typical length scale, cf. Eq. (2)], then the yield stress for solids at different dimensionless densities ρ was shown to vary like

$$\sigma_Y \approx \frac{\varepsilon}{\lambda^d} \rho^\nu, \quad \nu = 1 + \alpha/d. \tag{1}$$

It had been shown [5] that this scaling law is not valid in general when the interparticle potential contains an attractive part, except at very high densities when the particles are squeezed against the repulsive part of the potential. The aim of this paper is to provide a scaling theory that remains valid for generic potentials with an attractive and a repulsive part.

II. SYSTEM AND POTENTIALS

We investigate a binary system where the amount of bidispersity of "small" and "large" particles was chosen to guarantee that the models produce good glass formers both in two and three dimensions. We constructed a template for interparticle potentials where the microscopic lengths can easily be tuned:

$$\phi\left(\frac{r_{ij}}{\lambda_{ij}}\right) = \begin{cases} 4\varepsilon\left[\left(\frac{\lambda_{ij}}{r_{ij}}\right)^{12} - \left(\frac{\lambda_{ij}}{r_{ij}}\right)^6\right], & \frac{r_{ij}}{\lambda_{ij}} \leqslant \frac{r_{\min}}{\lambda} \\ \varepsilon\left[a\left(\frac{\lambda_{ij}}{r_{ij}}\right)^{12} - b\left(\frac{\lambda_{ij}}{r_{ij}}\right)^6 + \sum_{\ell=0}^{n} c_{2\ell}\left(\frac{r_{ij}}{\lambda_{ij}}\right)^{2\ell}\right], & \frac{r_{\min}}{\lambda} < \frac{r_{ij}}{\lambda_{ij}} < \frac{r_{\text{co}}}{\lambda} \\ 0, & \frac{r_{ij}}{\lambda_{ij}} \geqslant \frac{r_{\text{co}}}{\lambda} \end{cases} \tag{2}$$

where $r_{\min}/\lambda_{ij}$ is the length where the potential attains its minimum, and $r_{\text{co}}/\lambda_{ij}$ is the cutoff length for which the potential vanishes. The coefficients a, b, and $c_{2\ell}$ are chosen such that the repulsive and attractive parts of the potential are continuous with two derivatives at the potential minimum, and the potential goes to zero continuously at $r_{\text{co}}/\lambda_{ij}$ with two continuous derivatives as well. To satisfy the latter constraints it suffices for n to be equal to 3. In other cases

where r_{co} is fixed and we want to control the shape of the attractive part of the potential, $n = 4$. The interaction length scale λ_{ij} between any two particles i and j is $\lambda_{ij} = 1.0\lambda$, $\lambda_{ij} = 1.18\lambda$, and $\lambda_{ij} = 1.4\lambda$ for two "small" particles, one "large" and one "small" particle, and two "large" particles, respectively. The unit of length λ is set to be the interaction length scale of two small particles, ε is the unit of energy, and $k_B = 1$.
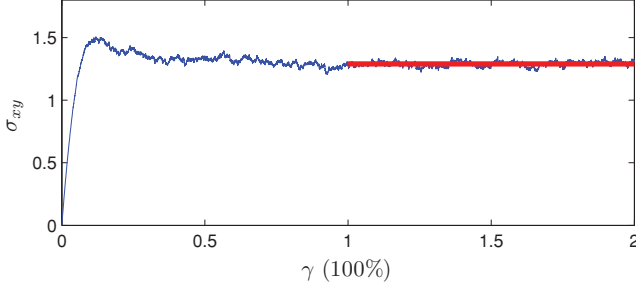
FIG. 1. (Color online) A typical stress vs strain curve. At low strains the stress increases linearly with the slope being the shear modulus. At a strain value of the order of 10% the system undergoes a yielding transition [4]. σ_Y is the mean stress computed at the elastoplastic steady state obtained after, say, 100% strain (see thick red curve).

III. METHODS

The work presented here investigates systems under simple shear in the athermal quasi-static limit, $T \rightarrow 0$ and $\dot{\gamma} \rightarrow 0$, where $\dot{\gamma}$ is the strain rate. AQS methods have been extensively used recently [6–11] as a tool for investigating plasticity in amorphous systems. The order in which the limits $T \rightarrow 0$, $\dot{\gamma} \rightarrow 0$ are taken is important, since one expects that at any finite temperature the stress in the system can thermally relax given long enough time [12] (or small enough strain rates), hence the limit $T \rightarrow 0$ should be taken prior to the $\dot{\gamma} \rightarrow 0$ limit. According to AQS methods, starting from a completely quenched configuration of the system, we apply an affine simple shear transformation to each particle i in our shear cell, according to

$$r_{ix} \rightarrow r_{ix} + r_{iy}\delta\gamma, \quad r_{iy} \rightarrow r_{iy}, \quad (3)$$

in addition to imposing Lees-Edwards boundary conditions [13]. The strain increment $\delta\gamma$ plays a role analogous to the integration step in standard molecular dynamics simulations. We choose for the discussed systems $\delta\gamma = 5 \times 10^{-5}$, which is sufficiently small for the analysis of the steady-state mean values. The affine transformation Eq. (3) is then followed by the minimization [14] of the potential energy under the constraints imposed by the strain increment and the periodic boundary conditions.

IV. THE YIELD STRESS IN TWO DIMENSIONS

We prepared systems with density ρ ranging in the interval [0.775, 0.935] with increments of 0.02. The low boundary of this interval is determined by retaining positive pressure in our simulation box for any of the considered microscopic lengths. For lower densities the system becomes porous with patches of vacuum, and we do not investigate such states. The range of the microscopic lengths considered to generate the various potentials is

$$r_{\text{co}} = 1.2\lambda_{ij} \times 1.06^k \quad \text{where} \quad k \in \{0, \dots, 12\}. \quad (4)$$

The microscopic lengths used to generate our data set of σ_Y values include all combinations of r_{co} and ρ with $n = 3$. A few examples of the different potentials can be seen in Fig. 2, panel A. Each such system with $N = 500$ particles was strained in
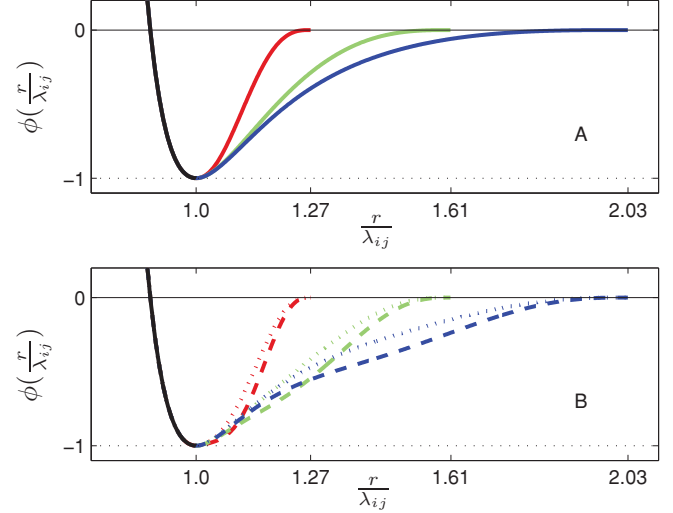

FIG. 2. (Color online) A selection of different potentials used to determine the yield stress. Panel A depicts potentials where $r_{\text{co}}/\lambda_{ij}$ is the changing length (increasing from left to right). Panel B shows potentials for which $r_{\text{co}}/\lambda_{ij}$ remains unchanged as in panel A but with a different attractive behavior.

AQS conditions and a typical result for stress-strain curves with given ρ is shown in Fig. 3. The yield stress in simulations are read from the steady-state stress-strain curve as depicted in Fig. 1. To understand these σ_Y values, we note that for a finite cutoff length the density determines how many neighboring particles are within the interaction length, and σ_Y is expected to be a strong function of the density. In the limit $r_{\text{co}} \rightarrow \infty$ all the particles are within the interaction range and the dependence on the density disappears in favor of a limiting value of $\sigma_Y \rightarrow \tilde{\sigma}_Y$.

To collapse the data on a single graph we note that there are three independent lengths in this problem, namely, λ, r_{co}, and $\tilde{\rho}^{-1/d}$. These three lengths render two ratios, i.e., $s_1 \equiv$
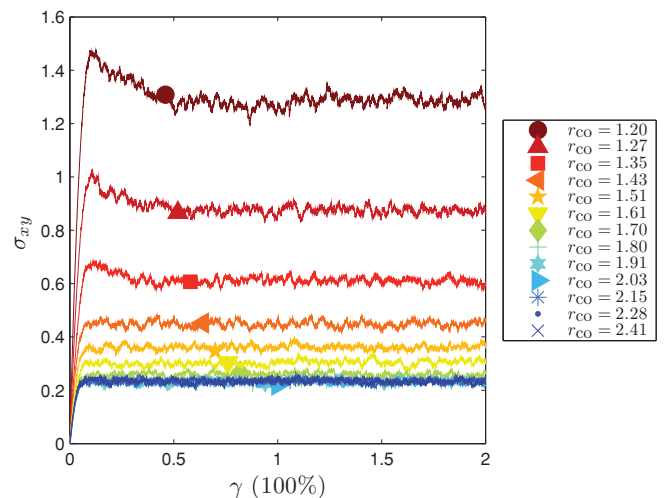

FIG. 3. (Color online) Stress vs strain curves in two-dimensional systems with the potential shown in Fig. 2, panel A. Note the convergence with increasing r_{co}.
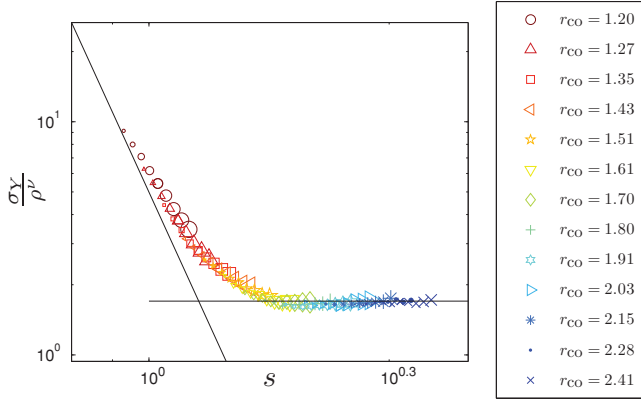
FIG. 4. (Color online) The scaling function $f(s)$ [cf. Eq. (6)], obtained by collapsing the computed σ_Y values in 2D. Smaller symbols represent lower densities. Potentials used here are of the type found in Fig. 2, panel A.

$\lambda/\tilde{\rho}^{-1/d} \equiv \rho^{1/d}$ and $s_2 \equiv r_{co}/\tilde{\rho}^{-1/d}$. In general one expects a scaling law with these two variables:

$$\sigma_Y = \frac{\varepsilon}{\lambda^d}\rho^\nu g(s_1, s_2). \tag{5}$$

We expect that the limit $s_1 \to \infty$ should reproduce the high-density limit Eq. (1). In contrast, we expect that $s_2 \to \infty$ should lead to the converged large interaction limit $\tilde{\sigma}_Y$. Thus these two dimensionless numbers work in opposite directions, and we consider the dimensionless product $s = s_1 \times s_2$ in which the effects of both ratios can balance. These consideration lead to a scaling ansatz in the form

$$\sigma_Y = \frac{\varepsilon}{\lambda^d}\rho^\nu f(s). \tag{6}$$

Here the scaling function $f(s)$ is expected to behave according to

$$f(s) = \begin{cases} \text{const} & \text{for} \quad s \to \infty, \\ s^{-\nu} & \text{for} \quad s \to 0. \end{cases} \tag{7}$$

Indeed, plotting σ_Y/ρ^ν as a function of s leads to a superb data collapse, as one can see in Fig. 4.

It should be noted that the choice of the scaling variable $s = s_1 \times s_2$ can be directly validated by checking that the value of σ_Y/ρ^ν is indeed invariant for a given s for any s_1 and $s_2 = s/s_1$; see Fig. 5. In the figure we plot the scaling function $f(\tilde{s} = \tilde{s}_1 \times \tilde{s}_2)$ vs $f(s = s_1 \times s_2)$ for a series of different values of s such that $\tilde{s}_1 \times \tilde{s}_2 \approx s_1 \times s_2$.

V. THE YIELD STRESS IN THREE DIMENSIONS

A sensitive test of the above-mentioned scaling theory is provided by validating the explicit dimensionality dependence. To this end similar data were collected for samples in three dimensions using the potentials with $n = 3$ and varying r_{co} values, see Eq. (4), combined with densities in the interval [0.76,1] with increments of 0.03 (emanating from the above-mentioned considerations). The beautiful scaling collapse in Fig. 6, simply changing the numerical value of ν as dictated by Eq. (1), confirms the choice of scaling function, Eq. (6).
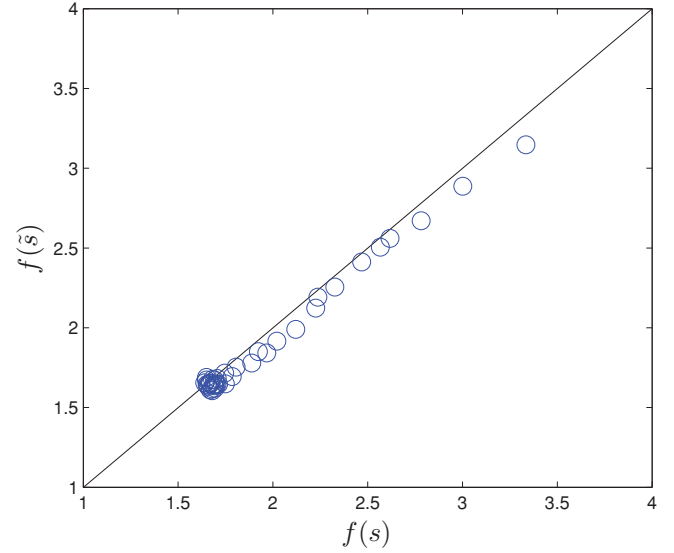

FIG. 5. (Color online) Plotted are the values of $f(s)$ vs $f(\hat{s})$ from the data set presented in Fig. 4, where $\frac{\hat{s}}{s} \approx 1$.

VI. THE EFFECT OF POTENTIAL SHAPE ON THE YIELD STRESS IN TWO DIMENSIONS

We have so far been successful in identifying the crucial microscopic lengths involved in determining the yield stress. The role of a change of shape in the attractive part of the potential now remains to be elucidated. (However, regardless of the shape of the potential we expect the limiting values to remain unchanged. In other words, we still expect that the limit $s_1 \to \infty$ should reproduce the high-density limit and that $s_2 \to \infty$ should lead to the converged large interaction limit $\tilde{\sigma}_Y$.) To this end we used two variations of potentials with $n = 4$ and r_{co} as in Eq. (4). For examples of such potentials see Fig. 2, panel B.

The change in physics as a result of changing the shape of the attractive part of the potential can be easily understood. As the potential well widens, the slope of the potential on the way to r_{co} increases. As long as the second shell of particles is *outside* the interaction range, the system softens as a result of the widening well. As soon as r_{co} reaches a value that *includes*
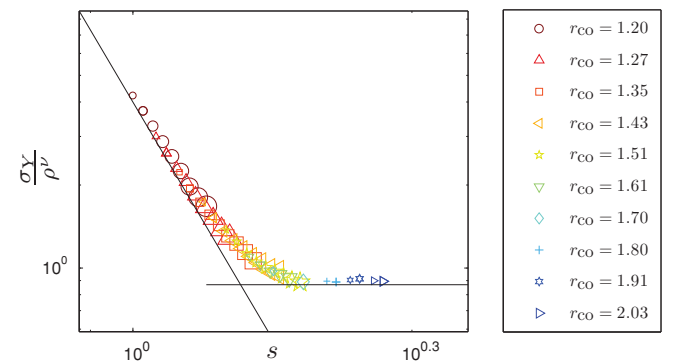

FIG. 6. (Color online) The scaling function $f(s)$ [cf. Eq. (6)], obtained by collapsing the computed σ_Y values in three dimensions using potentials as in Fig. 2, panel A, and $N = 1000$. Smaller symbols represent lower densities.
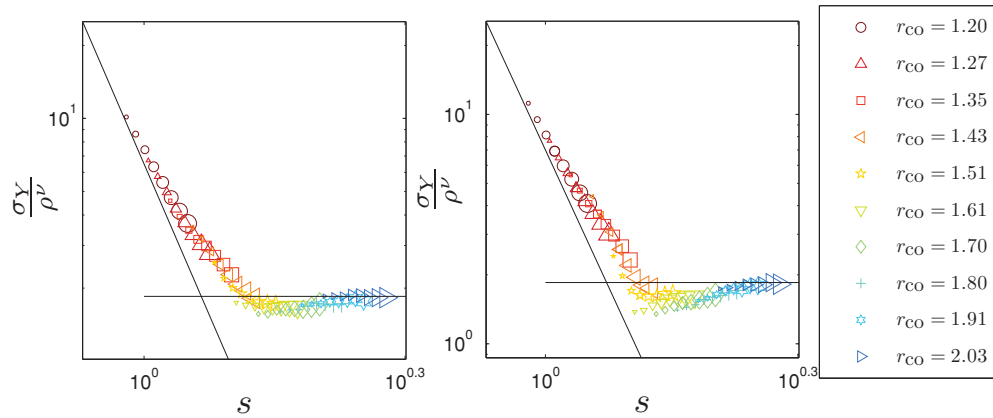
FIG. 7. (Color online) The scaling function $f(s)$ (cf. Eq. (6)), obtained by collapsing the computed σ_Y values in 2D. Smaller symbols represent lower densities. Left panel is the collapse of σ_Y values computed using the "dotted" fashion potentials appearing in Fig. 2, panel B, and the right panel is the collapse of σ_Y values computed using the "dashed" fashion potentials in the same panel.

the second shell, the strong attractive forces stiffen the system, thus creating a dip in the scaling function.

To corroborate this picture we repeated the AQS straining experiments for the altered potentials (see lower panel of Fig. 2 at similar densities as before in two dimensions). In Fig. 7 we see the unchanging asymptotes of the scaling function and the expected dip in σ_Y/ρ^ν. Note the larger dip in the right panel of Fig. 7. Note that this effect of softening and then hardening is always present, even if it is barely noticeable [15].

VII. CONCLUDING REMARKS

We have presented a scaling theory of the yield stress in AQS conditions, stressing the data collapse, and therefore of the high predictability of the scaling theory, when the potentials

are changing widely both in their shape and in the cutoff scale. The data collapse means that measuring the data for one potential we can predict how the yield stress will change for other potentials. Together with the recent scaling theory for the flow stress as a function of temperature and strain rate (albeit at this point only for purely repulsive potentials [5]), we begin to see a powerful theory based on scaling concepts that is emerging for the discussion of plasticity in amorphous solids.

[1] C. A. Schuh, T. C. Hufnagel, and U. Ramamurty, Acta Mater. **55**, 4067 (2007).

[2] F. Varnik, L. Bocquet, and J.-L. Barrat, J. Chem. Phys. **120**, 2788 (2004).

[3] D. Rodney and C. A. Schuh, Phys. Rev. B **80**, 184203 (2009).

[4] S. Karmakar, E. Lerner, and I. Procaccia, Phys. Rev. E **82**, 055103(R) (2010).

[5] E. Lerner and I. Procaccia, Phys. Rev. E **80**, 026128 (2009).

[6] C. Maloney and A. Lemaître, Phys. Rev. Lett. **93**, 016001 (2004).

[7] A. Tanguya, F. Leonforte, and J.-L. Barrat, Eur. Phys. J. E **20**, 355 (2006).

[8] C. E. Maloney and A. Lemaître, Phys. Rev. E **74**, 016118 (2006).

[9] N. P. Bailey, J. Schiøtz, A. Lemaître, and K. W. Jacobsen, Phys. Rev. Lett. **98**, 095501 (2007).

[10] E. Lerner and I. Procaccia, Phys. Rev. E **79**, 066109 (2009).

[11] M. Tsamados, A. Tanguy, F. Léonforte, and J.-L. Barrat, Eur. Phys. J. E **26**, 283 (2008).

[12] J-P. Eckmann and I. Procaccia, Phys. Rev. E **78**, 011503 (2008).

[13] M. P. Allen and D. J. Tildesley, *Computer Simulations of Liquids* (Oxford University Press, Oxford, United Kingdom, 1991).

[14] A variant of the conjugate gradient algorithm was used, for details see [http://www.inference.phy.cam.ac.uk/mackay/c/macopt.html].

[15] Note that slight increase in σ_Y for the largest value of r_{co} in Fig. 3. This is due to the influence of second shell neighbors entering the interaction range.